Combined loading capacity of skirted circular foundations in loose sand

Combined loading capacity of skirted circular foundations in loose sand

Manuscript submitted to Ocean Engineering on 17 April 2018 by:

Nicole Fiumana (corresponding author) [*]
PhD candidate
Email: nicole.fiumana@research.uwa.edu.au

Britta Bienen [*]
Associate Professor
Email: britta.bienen@uwa.edu.au

Laura Govoni [+]
Researcher
Email: l.govoni@unibo.it

Susan Gourvenec [*] [(^)]
Professor
Email: susan.Gourvenec@southampton.ac.uk

Mark J. Cassidy [*] [(#)]
Professor
Email: mark.cassidy@unimelb.edu.au

Guido Gottardi[+]
Professor
Email: guido.gottardi2@unibo.it

[*]Centre for Offshore Foundation Systems and ARC CoE for Geotechnical Science and Engineering
The University of Western Australia
35 Stirling Hwy
Crawley, Perth, WA 6009
Australia
Fax: +61 (0) 8 6488 1044

[+] DICAM
University of Bologna
Viale Risorgimento, 2
40125, Bologna
Italy

Formerly [*], now [^] Faculty of Engineering and Physical Sciences
University of Southampton, UK
+44 (0)23 80599139

Formerly [*], now [#] Melbourne School of Engineering
The University of Melbourne
+61 383446619

No. of words: 4554 (excluding abstract, references and figures)
No. of tables: 5
No. of figures: 14

Abstract

Skirted foundations are an attractive alternative foundation concept in the offshore energy sector, both for wind turbines and oil and gas platforms. Most of the evidence of skirted foundation behaviour under combined vertical, horizontal and moment (VHM) loading in sand has been collected from small-scale model experiments conducted at unit gravity on the laboratory floor. This paper presents results from a series of centrifuge experiments of skirted foundations on loose silica sand at relevant prototype stress levels. The vertical load-penetration curve is shown to be predicted well using established analytical methods. Centrifuge modelling results provide experimental evidence of the complex effects of the interaction of skirt aspect ratio and relative stress level on the VHM yield surface. A conservative and design-oriented solution based on the yield envelope approach describes available foundation capacity within the established framework of strain-hardening plasticity theory.

Key words: Skirted foundation; capacity; combined loading; centrifuge modelling; sand.

INTRODUCTION

Skirted foundations find wide application offshore for both fossil and renewable energy installations. Traditionally employed in fine grained seabeds for oil and gas facilities (Christophersen 1993), their use has been extended to jacket supported structures in sandy seabeds (Bye et al. 1995). Shallowly embedded skirted foundations offer a convenient solution as foundations for jack-up units, either as an alternative or in combination with spudcan foundations (e.g. Vlahos et al. 2006; Bienen et al. 2012; Vulpe et al. 2013; Cheng & Cassidy 2016). Skirted foundations have been also considered as a cost-effective alternative to monopiles in supporting wind turbines (e.g. Borkum Riffgrund 1 in the North Sea and 71 Aberdeen Offshore Wind Farm off the east coast of Scotland), in the form of suction caissons either as a monopod or in a group of three or four foundations of a jacket (e.g. Byrne & Houlsby 2002; Houlsby, et al., 2005; Houlsby 2016; Tjelta 2015). Different uses of skirted foundations in the offshore environment are shown schematically in Figure 1. Figure 1a and Figure 1b depict a monopod and jacket arrangement for wind turbines while Figure 1c and Figure 1d illustrate a jack-up unit and jacket structure, respectively. Skirted foundations can vary in diameter from about 6 m to 8 m for a jacket supported offshore wind turbine to a range of 10 m to 20 m for oil and gas jackets, monopod supported offshore wind turbines and jack-ups. The aspect ratio of the skirt length d to diameter D is generally less than 1 m in sand, with d/D of 0.25 or less required in jack-ups to ensure the skirts can be lifted back inside the holding for redeployment.

Significant horizontal load (H) and overturning moment (M) characterise load paths of offshore foundations. In general, actions on skirted foundations for wind turbines are characterised by low values of vertical load (V), compared to those of oil and gas platforms. Bearing pressures V/A, where A is the plan area of the foundation, generally range between 40 to 125 kPa (Byrne et al. 2002; Houlsby & Byrne 2005) in offshore wind applications, and 300 to 760 kPa (Cassidy et al. 2004; Bienen et al. 2009) in oil and gas installations. The capacity of foundations to withstand combined vertical (V), horizontal (H) and moment (M) loading can be conveniently expressed in terms of a yield surface.

Early investigations of the yield surface of foundations in sand were based on data of single gravity experiments on small flat plates in dense (Gottardi et al. 1999) and loose

sand (Nova & Montrasio 1991; Gottardi & Butterfield 1995; Bienen et al. 2006; Bienen et al. 2007). These studies made extensive use of the swipe testing procedure that was first used by Tan (1990) to track a path along the yield surface in a single experiment. The test results consistently suggested that the yield surface of a shallow foundation expands with mobilised vertical load (V_0), which can be uniquely described in normalised load space (normalising the load axes by V_0) by the following equation (Gottardi et al. 1999)

$$\left(\frac{M/D}{m_0 V_0}\right)^2 + \left(\frac{H}{h_0 V_0}\right)^2 - 2\alpha \frac{HM/D}{m_0 h_0 V_0^2} - {\beta_{12}}^2 \left(\frac{V}{V_0}\right)^{2\beta_1} \left(1 - \frac{V}{V_0}\right)^{2\beta_2} = 0 \qquad \text{Eq. 1}$$

where β_1 and β_2 are shape parameters influencing where the peak horizontal and moment loads occur under vertical load, and $\beta_{12} = \frac{(\beta_1+\beta_2)^{(\beta_1+\beta_2)}}{{\beta_1}^{\beta_1}{\beta_2}^{\beta_2}}$. The coefficients m_0 and h_0 control the size of the yield surface in the moment and horizontal load plane respectively.

Eq. 1 has been shown to accurately represent the yield surface of shallow surface foundations at prototype stress conditions, as demonstrated through a series of centrifuge swipe tests on flat plates on medium dense sand (Cassidy 2007; Govoni et al. 2010; Cheng & Cassidy 2016) and tests of a full jack-up platform with three conical spudcan foundations on dense sand (Bienen et al. 2009).

The effect of the skirt length on the yield surface in drained conditions on sand was first addressed with reference to bucket foundations of different embedment ratios (skirt length d to diameter D) (d/D = 0, 0.166, 0.33, 0.66) on very dense sand samples (Byrne & Houlsby 1999; Byrne 2000). Single gravity tests, mostly of the swipe type, were carried out at low values of vertical load $V_0 \leq 0.25 \leq V_{peak}$, where V_{peak} identifies the value of the peak vertical bearing capacity, with results showing that the normalised yield surface increases (i.e. h_0 and m_0 become larger) with decreasing V_0/V_{peak}. At low vertical load the response deviates from the parabolic yield surface shape to follow a frictional sliding surface, dilatant in the presence of dominant overturning moment (M) and contractant when the horizontal component of the load (H) is dominant. This concept of the yield surface is illustrated in Figure 2a, in planes containing the vertical load (V) axis. A similar dependency of the normalised yield surface shape and size on the load path was also exhibited by spudcan foundations subjected to swipe tests on sand in the centrifuge

(Cheng 2015; Cheng & Cassidy 2016a). Results of centrifuge swipe tests on flat plates buried in medium dense sand samples also displayed a similar pattern, which included a high non-vertical load capacity at low and even negative values of the vertical load (Govoni et al. 2011). Non-zero horizontal and moment capacity in the tensile range of the vertical load was also shown in results of skirted foundation model tests under combined loading on loose sand at 1g (Villalobos 2006). In order to accommodate the experimentally observed behaviour, Villalobos et al. (2009) expressed the yield surface as follows and as qualitatively represented in Figure 2b.

$$\left(\frac{M/D}{m_0 V_0}\right)^2 + \left(\frac{H}{h_0 V_0}\right)^2 - 2\alpha\frac{HM/D}{m_0 h_n V_0^2} - {\beta_{12}}^2\left(\frac{V}{V_0} + t_0\right)^{2\beta_1}\left(1 - \frac{V}{V_0}\right)^{2\beta_2} = 0 \qquad \text{Eq. 2}$$

where t_0 is defined as the yield surface tension parameter.

A similar expression for the yield surface was recently used to interpret the combined loading response of a skirted foundation on dense sand based on evidence from 1g experiments (Foglia et al. 2015).

A summary of the experimental research on the VHM yield surface of shallow foundations on sand is given in Table 1.

Though these studies have shown that foundation embedment has a marked influence on the VHM yield surface, particularly at low values of vertical load mobilisation (V_0), evidence at prototype stress levels is lacking. This study therefore aims to close the gap in providing centrifuge experimental evidence of the VHM yield surface of circular skirted foundations in sand investigating the effect of two different skirt aspect ratios (d/D = 0.25 and d/D = 0.5) on the horizontal and moment capacity. Both high and low stress levels reflective of the prototype are considered. The specific contributions of this paper are:

- new experimental evidence on the vertical and combined planar VHM loading response of skirted foundations on sand at stress levels reflective of the prototype;
- insights into the effects of skirt aspect ratio (d/D) and stress level on the horizontal and moment capacity;

- recommendations for the assessment of VHM capacity of skirted foundations in sand in practice.

EXPERIMENTAL SET-UP AND PROCEDURE

Drum centrifuge, VHM actuator and model foundation

The experiments were carried out in the 1.2 m diameter drum centrifuge at the University of Western Australia (Stewart et al. 1998). The soil model is contained in the drum channel, which is 0.3 m wide and 0.2 m deep. Two concentric shafts allow independent control of the drum and testing instruments connected to the central actuator.

An in-house developed VHM apparatus (Zhang et al. 2013) was used in the experiments. The vertical, horizontal and rotational foundation displacements are applied by movement of two actuators, which are linked as shown in Figure 3. The movement is transferred to the foundation via an instrumented tubular section, which is strain-gauged to measure vertical as well as moment loading in two locations. This allows the vertical, horizontal and moment load at a reference point (RP) on the foundation to be determined, assuming linear variation of the bending moment. Any combination of vertical, horizontal and rotational movement (as defined in Figure 3) of the foundation reference point (within the scope of the VHM actuator) can be prescribed to be independently controlled, with a rotational component requiring simultaneous compensations in vertical and horizontal movements (Figure 4). Further details on the apparatus can be also found in Cheng and Cassidy (2016).

Two foundation models, fabricated from aluminum, were used in the experiments. The foundation diameter D was 50 mm in both models, representing a prototype diameter of 5 m when tested at 100 g. One model featured a skirt length d of 12.5 mm, resulting in an aspect ratio d/D = 0.25, the other had a skirt length of 25 mm giving an aspect ratio d/D = 0.5. The skirt thickness t was 1 mm, selected to ensure sufficient robustness to ensure against buckling during installation and combined load testing. The models (shown in Figure 3) were provided with an electronic venting system chosen to enable in-flight installation and sealing. The seal was remotely actuated once the lid came in contact with

the soil. The venting system ensured no water was trapped inside the skirt compartment of the penetrating foundation and hence no significant excess pore pressure could occur during installation within the plug.

Soil sample

The experiments were performed in commercially available silica sand, which is routinely used at UWA. Table 2 summarises the sand properties (Liu & Lehane 2012). The sample was prepared by pluviation through 165 mm of water while the centrifuge was spinning at 20g. Once the raining process was complete, the water was drained out of the channel, the centrifuge was stopped and a plastic scraper was used to level the surface. The final sand sample height was 150 mm. The sample was resaturated in flight over night prior to testing.

The sample preparation procedure produced a loose soil sample, characterised through miniature cone penetrometer tests (CPT) with a cone diameter of 6 mm. Tests were carried out at various locations around the sample. The penetration rate of the cone was 0.1 mm/s. Figure 5 shows a representative CPT result in terms of cone tip resistance q_c and dimensionless net tip resistance q_{net} with penetration w and normalised penetration w/D, respectively, where D is the diameter of the skirted foundation.

$$q_{net} = (q_c - \sigma_{v0})/\sigma'_{v0} \quad \text{Eq. 3}$$

An average relative density D_r of 30% was derived from the experimental results according to the relationship (Schneider & Lehane, 2006).

$$D_r = 100(q_{net}/250)^{0.5} \quad \text{Eq. 4}$$

The effective unit weight was computed from mass measurements of the sample and returning a value of $\gamma' = 10$ kN/m^3.

Experimental strategy and testing program

The experimental program comprised a series of vertical penetration and swipe tests. Vertical penetration tests were carried out with and without unload-reload cycles on both foundation models to obtain the evolution of uniaxial capacity with foundation penetration and an indication of vertical unloading stiffness. The vertical load-penetration tests allowed selection of the target penetration depths at which swipe tests were performed.

Swipe tests formed the majority of events included in this centrifuge testing program.

In order for the centrifuge tests to reflect prototype behaviour, both foundation penetration and swipe tests need to be performed at enhanced gravity. The footing was installed at 100g with the vent open. When the lid invert came into contact with the soil surface, the valve was closed. The entire procedure was executed without stopping the centrifuge. In swipe tests, the foundation was further penetrated to the target vertical displacement (w_0). The vertical load mobilised at this point is termed V_0. The vertical displacement was then held constant while horizontal displacement (u), rotation (θ) or a constant combination of the normalised ratio u/Dθ were applied to the foundation RP. The swipe tests commenced immediately after reaching the target penetration, so that there were no delays causing relaxation and leading to the load paths lying inside, rather than tracking the VHM yield surface (Bienen et al. 2007). The RP was located at the underside of the foundation base plate (Figure 3), similar to previous experiments under drained conditions (e.g. Villalobos 2006). The tests were performed entirely under displacement control at a model rate of 0.1mm/s in all directions so as a drained soil response was ensured (Cheng & Cassidy 2016b). All swipe tests commenced from V_0, without unloading.

Two values of vertical penetration were targeted in the experiments (w_0 = 0.6D; 0.3D, Table **3**), corresponding to low and high values of vertical bearing pressure V/A of 100 kPa and 500 kPa, respectively. These bearing pressures are relevant to the offshore energy installations shown in Figure 1. For each target stress level and skirt length of the foundation model, four different displacement ratios u/Dθ were investigated in order to obtain sufficient evidence of the VHM yield surface in three-dimensional space. The experimental program included 16 swipe tests, which are summarized in Table 3.

RESULTS AND DISCUSSION

Presentation of results and notation

The experimental results are presented in prototype dimensions V, H, M, w, u, Dθ, respectively for load and displacements, and normalised quantities to allow comparisons. The normalisation for the vertical displacements is w/D, while for the load components a selection of normalisations are adopted, according to the stress level V/A, V/Aγ'(d+D/2), V/$\pi\gamma'$(D^3/8) and to the reference load for the interpretation of the swipe tests, V/V_0, H/V_0, M/DV_0.

Vertical load-penetration curve

The vertical load-penetration curves are presented in Figure 6a, including the dedicated tests with and without unload-reload loops on both foundation models as well as the initial vertical loading phase of all swipe tests. The results also serve to confirm uniformity of the soil sample, as the data for each of the two foundation models are tightly grouped.

The penetration resistance increases approximately linearly initially as the skirts penetrate the sand. The gradient of the penetration resistance changes markedly as the lid invert comes into contact with the soil. At this point the bearing pressure V/A is approximately 100 kPa for the foundation with the aspect ratio d/D = 0.25 and 245 kPa for d/D = 0.5.

The obtained load-displacement relationship demonstrates the characteristic response of foundation penetration in loose sand, with bearing capacity increasing monotonically with penetration. The target penetration depths selected to achieve the desired stress levels at the commencement of the swipe tests are indicated in Figure 6a.

Normalisation of the bearing pressure by the soil self-weight stress level half a diameter below the skirt tip as proposed in Govoni et al. 2011, unifies the measured response of the two aspect ratios as shown in Figure 6b.

The observed response during skirt penetration is well predicted using the bearing capacity based approach outlined in Houlsby and Byrne (2005) as the sum of the friction

developing in the inner (i) and outer (o) part of the skirt and the bearing resistance of the skirt annulus (Eq. 5). The linear prediction is plotted in terms of normalised quantities in Figure 6b with reference to the foundation with a ratio d/D = 0.25.

$$V = \frac{\gamma' w^2}{2}(K\tan\delta)_o(\pi D_o) + \frac{\gamma' w^2}{2}(K\tan\delta)_i(\pi D_i) + \left(\gamma' w N_q + \gamma' \frac{t}{2} N_\gamma\right)(\pi A_{tip}) \quad \text{Eq. 5}$$

Villalobos (2006) suggests the use of the Rankine passive coefficient K = (1+sinφ)/(1-sinφ) to be a good approximation for the analysis of the skirt penetration for the case of a smooth skirt. The drained bearing capacity factors were computed with the software ABC (Martin 2003) for a surface strip foundation (Villalobos 2006) of breadth B = D resting on sand (γ' = 10 kN/m3 and φ = 31°) and equal to N_q = 20.90 and N_γ = 17.95. The frictional properties considered for the sand refer to a friction angle, φ = 31° and an interface friction angle between the soil and the skirt wall, δ = 2 /3 φ = 21°. In the present study, the enhancement of stress due to the frictional forces close to the skirt wall was not taken into account, which would instead represent a more conservative solution (Houlsby & Byrne 2005). However, Figure 6 shows the prediction using Eq. 5 to be consistent with the experimental results.

Alternatively, the model proposed by Andersen et al. 2008 also provides a good estimation of the skirt penetration behaviour, which uses a smaller K value, but includes the effect of the additional stress on the tip resistance. The parameters Nq and Nγ were selected equal to 74 and 95 respectively as related to field model tests more similar to the herein prototype (Andersen et al. 2008) and K=0.8 (Figure 6b). Details on the equation can be found in Andersen et al. 2008.

Figure 6b also reports the drained bearing capacity prediction from the software ABC (Martin 2003), considering a smooth circular foundation of 5 m diameter on a soil with γ' = 9.94 kN/m^3 and $\varphi' = 31°$. The penetration was simulated by computing the bearing pressure for increasing values of overburden pressure q. The touchdown value and the non-linearity of the behaviour during penetration result was slightly overestimated (20%) with respect to the experimental data. This could be due to the assumption of an associated flow in the limit analysis program which is known to lead to over-prediction of vertical bearing capacity in sand. Another possibility is the gradual mobilisation of resistance in

the physical experiment, which is in contrast with the instantaneous full resistance modelled numerically. This method, however, provides a closer reproduction of the response with respect to buried footings or spudcan hardening laws (Govoni et al. 2011; Cheng & Cassidy 2016).

The hardening laws for buried (Govoni et al. 2011) and spudcan foundations (Cheng & Cassidy 2016a) are included in Figure 6b for comparison. The adopted relationship to describe the pure plastic response of the skirted foundations under monotonic vertical loads was that proposed by Bienen et al. (2006) and rewritten in terms of dimensionless parameters (Govoni et al. 2011):

$$\frac{V}{(A\sigma'_v)} = \left(\frac{DK_1}{A\sigma'_v}\right)\frac{w_p}{D}\left[\frac{1+\frac{w_p}{D}\left(\frac{D}{w_1}\right)}{1+\frac{w_p}{D}\left(\frac{D}{w_2}\right)}\right] \qquad \text{Eq. 6}$$

where the best fit coefficients are: $(Dk_1)/(A\sigma'_V) = 19417.6$, $w_1/D = -1.16$, $w_2/D = 2.23$ and where $(Dk_1)/(A\sigma'_V)$ represents the dimensionless stiffness, with $\sigma'_V = \gamma'(d + D/2)$ (Bolton & Lau 1988).

Incorporation of unload-reload loops into vertical load-penetration tests provide an indication of the elastic stiffness of the soil-foundation system. Obtained values are plotted in Figure 7 against the related stress level. The normalised form $Dk_e/A\sigma'_v$ allows comparison with obtained values for a spudcan foundation on loose sand (Cheng & Cassidy 2016a) and buried foundations on medium dense sand (Govoni et al. 2011), showing a good agreement.

The unload stiffness can be also compared with theoretical solutions, for instance $K_v = \frac{V}{wGR}$ (Doherty & Deeks 2003). By assuming a representative shear modulus for the soil G = 13.8 N/mm^2 (Cheng & Cassidy 2016b), an average normalised stiffness $Dk_e/A\sigma'_v$= 1513 was obtained (Figure 7).

A value for the elastic stiffness of $Dk_e/(A\sigma'_{v0})$ = 1266 was used to plot the derived relationship for the plastic response (Eq. 6) in terms of total displacements. From the comparison with the hardening laws derived for a spudcan (Cheng & Cassidy 2016a) and

a buried foundation (Govoni et al. 2011) in Figure 6b, the response appears to be qualitatively similar. The scatter deriving from geometrical effects and higher density of the sample of the buried foundations (Figure 6), suggests neither equation is suitable for the description of the vertical penetration of skirted foundations.

Figure 8 compares the installation response obtained from 1g vertical penetration tests with those from the centrifuge test data of this study. The 1g data refer to the work of Villalobos (2006), and details of the test characteristics are provided in Table 4 in terms of d/D ratio, relative density of the sample, vertical load and displacement measured at full contact of the foundation lid with the soil. The comparison is presented first as bearing pressure – normalised displacement response (Figure 8a), which highlights the low stresses in the 1g tests, and secondly in the load normalisation proposed by Bolton and Lau (1989) (Figure 8b), with the specific purpose of comparing 1g and centrifuge tests. However, as the effect of stress level on the stiffness is not captured by this normalisation, it fails to unify the measured responses. This confirms the observations reported in Bienen et al. (2007) with a very stiff initial load-displacement response and enhanced mobilised friction angle due to increased dilatancy at the low stress levels at 1g and reinforces the importance of the stress state of the soil on foundation behaviour.

Capacity under combined VHM loading

In this section, the observed response during swipe tests dominated by moment and horizontal load, respectively, is discussed. Results of all swipe tests are then presented, with discussion of the effects of the level of vertical load and foundation aspect ratio on the VHM yield surface. The analysis is then discussed in terms of deviatoric components, before expressions to fit the foundation capacity are explored.

Response under predominantly horizontal or moment loading

Figure 9 shows results obtained for the four tests (combinations of d/D = 0.25, 0.5; V/A = 100, 500 kPa) executed with a displacement ratio $u/D\theta = -0.1$, resulting in a response dominated by moment. The response is in accordance with typical swipe results, with the vertical reaction decreasing as moment load increases, tracing a parabolic shape in the dominant VM plane. The horizontal load continues to increase, at low levels, in all tests

following an initial minimum (Figure 9a), and all tests exhibit a peak in moment capacity (Figure 9a and c). The tests of both foundation aspect ratios commencing from low V_0 ($\sim$100kPa) values exhibit strongly dilatant behaviour when the load paths leave the parabolic section of the yield surface (Figure 9b and d), but this is suppressed at high initial bearing pressure ($\sim$500kPa). In the case of a low foundation aspect ratio (d/D = 0.25) and high V_0, the peak moment is only marginally higher than the moment loading maintained for the remainder of the test (Figure 9a). The test with foundation of higher aspect ratio (d/D = 0.5), also at high V_0, results in slightly contractant behaviour in the V-M/D plane (Figure 9d). Similar observations were reported on the basis of 1g tests of skirted foundations on dense sand at low stress levels (Byrne 2000) and more recent centrifuge tests of spudcan foundations (Cheng & Cassidy 2016a).

Figure 10 shows results obtained for a group of tests executed with a displacement ratio $u/(D\theta) = \infty$, for which the horizontal load dominates the response. A similar observation to the previous example of a parabolic trace of the yield surface in the dominant loading plane (VH) is observed. Tests performed at high V_0 show a marked peak in the horizontal reaction, (with reference to prototype units), and appears more evident for the smaller aspect ratio (Figure 10a and c). A dilatant behaviour is evident in the test at low V_0 and d/D = 0.5 (Figure 10d), reached when the vertical reaction becomes negative. For low V_0 and small aspect ratio (Figure 10a) the test reaches a 'parallel point' (Tan 1990), after which the reactions remain constant despite increasing displacements. A parallel point is also observed for tests SW3, SW9 and SW11, performed at high V_0 (Figure 9a and 9c, Figure 10c).

All experimental results in the VH and VM planes

The obtained load response of all the swipe tests is presented in four pairs of plots, organised by the displacement ratio applied in the swipe event. These are presented in terms of prototype units in Figure 11 and normalised quantities in Figure 12.

The experimental results initially trace a parabolic yield surface before the load paths proceed along a sliding surface, with low stresses generally resulting in dilatant response. At higher stresses, the behaviour tends towards a parallel point. For the swipe

displacement ratio u/Dθ = 1.15 dilatant behaviour resulted independent of skirt aspect ratio and stress level, which is in contrast to tests subjected to horizontal displacement and rotation in opposing directions.

Figure 11 allows a better visual understanding of the effect of the skirt length on the capacity. Byrne (2000) observed that an increase in the skirt length leads to an increase in the yield surface only in the horizontal direction. This behaviour appears here more pronounced for swipe tests performed at low V_0.

The normalised load paths presented in Figure 12 further illustrate the common general trend in the shape of the yield surface, with some differences arising from the stress level and skirt length, depending on the load path. The centrifuge experimental evidence supports the concept of a family of yield surfaces, with elements of the expressions proposed by Byrne and Houlsby (999) and Villalobos et al. (2009) present (Figure 2). For the first two sets of displacement ratios (u/Dθ = ∞ and u/Dθ = -1.15) the swipe events terminate at $V/V_0 \leq 0$ in combination with non-zero values of horizontal or moment loads. This is not evident for flat foundations (Govoni et al. 2011) and suggests the foundation skirts enhance the yield surface to encapsulate also tensile loads. However, this does not seem to hold for the other displacement ratios and hence should not be relied on in the overall performance of the foundation.

All experimental results in the HM plane

Figure 13 compares the experimental results in the M/D vs H plane for a) d/D = 0.25 and b) d/D = 0.5. The data are presented in prototype units.

The load paths obtained by imposing the fixed displacement ratios on the swipe tests extend over two quadrants for all the tests. Displacement ratios $u/D\theta = \infty$ and $u/D\theta = -1.15$ present positive values of horizontal reaction, H, while the moment load component, M/D, starts negative, decreases to zero, and assumes positive values at the end of the swipe event. The tests dominated by moment $(u/D\theta = -0.1)$ in a similar way feature an initial negative horizontal reaction, ending with positive values.

The resulting load paths are quite complex, with a variable ratio of horizontal and moment loads developing during the swipe event, for constant displacement ratios applied. Swipe tests, in which similar displacement ratios were applied, display similar load paths initially, differing later depending on the level of vertical load applied. Greater skirt length (d/D = 0.5) leads to wider coverage of the load space, and later divergence of load paths depending on the vertical load level.

Representation of the results in the deviatoric planes

A convenient representation of such complex load paths can be obtained by projecting the load components in the deviatoric plane, described by the quantity $L = [H^2 + M/D^2]^{0.5}$. This approach does not require the size and shape of the capacity surface to be assumed and proved to be efficient for the interpretation of centrifuge data from surface and buried footings (Govoni et al. 2011). In a similar way, the displacement components can be represented in the combined form $[u/D^2 + \theta^2]^{0.5}$.

The obtained load displacement curves and load responses are presented in Figure 14, for each displacement ratio applied. In order to investigate the effect of the skirt aspect ratio, the load components, V and L, are normalised by $A\gamma'(d + D/2)$, which proved to be a convenient normalization for the interpretation of the penetration response. The load-displacement paths exhibit very consistent curves, in terms of shape and stiffness, with a clear peak followed by hardening.

The experimental load paths for the two aspect ratios, d/D = 0.25 and d/D = 0.5, are compared with the analytical expression of the yield surface proposed by Byrne and Houlsby (2001). The parameters were obtained from 1g tests of surface foundations in loose sand. This provides a relatively good fit to the shape of the swipe test results, particularly at high vertical loads, though the capacity is generally underestimated and some dependence on the loading mode is evident, similar to observations reported in Bienen et al. (2006). For $u/D\theta = \infty$ and $u/D\theta = -1.15$ (Figure 14 b and d) respectively, a non-negative deviatoric vertical load is observed, as already commented on for previous plots. For displacement ratios $u/D\theta = -0.1$ and $u/D\theta = 1.15$ (Figure 14 f and g) a transition point can be observed, with a sliding surface developing with a

constant slope, independent of the skirt length and vertical load level. The effect of the skirt length is particularly evident for $u/D\theta = -0.1$. The increase of the yield surface with increase in aspect ratio is unconnected to the stress level. From this representation emerges more clearly the dependence of the quality of the fit on the load path.

Description of VHM yield surface for skirted foundations in sand

All experimental swipe tests results are plotted in Figure 15 in terms of Q/V_0 vs V/V_0. This representation allows evaluation of the yield surface size and shape against the experimental data at one glance, rearranging Eq. 1, by combining the horizontal and moment load in the form:

$$Q = \sqrt{\left(\frac{(M/V_0)^2}{{m_0}^2}\right) + \left(\frac{(H/V_0)^2}{h_0}\right) - 2\alpha\frac{(M/V_0)(H/V_0)}{m_0 h_0}} \qquad \text{Eq. 7}$$

The capacity for the aspect ratio d/D = 0.25 is better captured by the fit proposed by Byrne and Houlsby (2001) than d/D = 0.5. An effect of the load path and stress level is also observed. This fitting suits best the displacement ratios $u/D\theta = \infty$ and $u/D\theta = -1.15$ and high stress levels.

In order to further compare the experimental data with the available sets of parameters, the fitting obtained for Villalobos et al. (2006) is presented in Figure 16. Even if the introduction of the tension factor could capture the potential tensile capacity of the foundations, this set of parameters is not able to adequately describe the response. In comparison to the parameter set suggested by Byrne and Houlsby (2001), the size of the yield surface, in particular in the horizontal direction (h_0), appears to be over-estimated by the parameter values provided in Villalobos et al. (2006). Further, the large negative eccentricity in the HM plane, defined by α, fails to unite the experimental results.

The best fit of the yield surface is described by a new set of parameters, reported in Table 5, with results presented in Figure 17. This is an improvement on the fitting obtained from Byrne and Houlsby (2001), and the best possible without introducing further complexity to the yield surface expression. For the design point of view, the suggested combination

of yield surface parameters (Table 5) provides a conservative approximation of the capacity for a foundation with aspect ratio d/D = 0.5 for some load paths (Figure 17b) whilst adequately accommodates the VHM capacity of the foundation with lower aspect ratio (Figure 17a). For the same reason of providing a conservative design approach, a tensile factor t_0 was not incorporated in the yield surface formulation, as the experimental evidence is insufficient for relying on the mobilisation of tensile capacity in design.

At lower stresses, the experimental data indicate h_0 and m_0 to be larger than suggested by the overall fit. This is in line with findings by Byrne and Houlsby (2001) and Govoni et al. (2011). The centrifuge experimental data require the eccentricity parameter α to be positive for the yield surface expression to provide a close fit. This contrasts with published recommendations for flat and spudcan foundations on sand but agrees with suggestions for foundations on clay. This is most probably due to the variation of soil strength over the depth that the skirted foundations mobilise the soil failure mechanism. A value of 1 for the shaping parameters β_1 and β_2 fits the data well overall. However, the yield surface shape shows some variation depending on the load path. Combinations dominant in horizontal loading require $\beta_2 < \beta_1$, i.e. a bias of the yield surface peak towards lower vertical load, whereas the converse holds for moment dominant load paths, with larger capacity available at high vertical loads than a yield surface with $\beta_1 = \beta_2$ describes, as seen in Figure 14.

CONCLUDING REMARKS

This work presents the results of centrifuge tests of skirted foundations in loose silica sand under combined VHM loading, with an emphasis on the effect of relative stress level and skirt aspect ratio on the shape and size of the yield surface. The results are compared with available previous studies on shallow skirted foundations at 1g and centrifuge tests on surface and spudcan foundations.

The findings indicate that the well-established framework of strain-hardening plasticity is relevant to skirted foundations in sand under prototype stress conditions. The experimental results indicate the level of vertical load, the skirt aspect ratio and the load

combination all influence the available capacity. A simplified description of the overall yield surface size and shape is provided.

Comparison with results from 1g test results underline the importance of modelling at stress levels relevant to prototype conditions for capturing the vertical load response accurately. Low stress levels characterising the 1g environment lead to an underestimation of the hardening response. In contrast, comparison of combined loading tests performed in the centrifuge environment with established yield surfaces in VHM load space based on 1g tests, results in good agreement.

ACKNOWLEDGEMENTS

This work forms part of the activities of the Centre for Offshore Foundation Systems (COFS). Established in 1997 under the Australian Research Council's Special Research Centres Program. Supported as a node of the Australian Research Council's Centre of Excellence for Geotechnical Science and Engineering, and through the Fugro Chair in Geotechnics, the Lloyd's Register Foundation Chair and Centre of Excellence in Offshore Foundations and the Shell EMI Chair in Offshore Engineering. The work presented was performed while the first author was a visiting scholar at COFS, UWA, supported by the University of Bologna and ARC grant FL130/0005. This support is gratefully acknowledged.

References

Andersen, KH, Jostad, HP, Dyvik, R 2008, 'Penetration resistance of offshore skirted foundations and anchors in dense sand'., *Journal of Geotechnical and Geoenvironmental Engineering*, vol 134, no 1.

Bienen, B, Byrne, BW, Houlsby, GT & Cassidy, MJ 2006, 'Investigating six-degree-of-freedom loading of shallow foundations on sand'., *Géotechnique*, vol. 56, no. 6, pp.367–379.

Bienen, B, Cassidy, MJ & Gaudin, C 2009, 'Physical modelling of the push-over capacity of a jack-up structure on sand in a geotechnical centrifuge'., *Canadian Geotechnical Journal*, vol. 46, pp.190–207.

Bienen, B, Gaudin, C & Cassidy, MJ 2007, 'Centrifuge tests of shallow footing behaviour on sand under combined vertical-torsional loading'., *International Journal of Physical Modelling in Geotechnics*, vol. 7, no. 2, p.0.1-21.

Bolton, MD & Lau, CK 1988, ‘‘Scale effects arising from particle size’’, *Proceeding of the International conference on geotechnical centrifuge modelling* , pp.127–131.

Byrne, BW 2000, *Investigations of suction caissons in dense sand*, University of Oxford.

Byrne, BW & Houlsby, GT 1999, ‘‘Drained Behaviour of Suction Caisson Foundations on Very Dense Sand’’, *1999 Offshore Technology Conference (OTC)* , Houston, TX.

Byrne, BW & Houlsby, GT 2001, ‘Observation of footing behaviour on loose carbonate sands’., *Géotechnique*, vol. 51, no. 5, pp.463–466.

Byrne, BW & Houlsby, GT 2002, ‘Suction Caisson Foundations for Offshore Wind Turbines and Anemometer Masts’., *Wind Engineering*, vol. 26, no. 3, pp.145–155.

Cassidy, MJ 2007, ‘Experimental observations of the combined loading behaviour of circular footings on loose silica sand’., *Géotechnique*, vol. 57, no. 4, pp.397–401.

Cassidy, MJ, Martin, CM & Houlsby, GT 2004, ‘Development and application of force resultant models describing jack-up foundation behaviour’., *Marine Structures*, vol. 17, no. 3, pp.165–193.

Cheng, N 2015, *Force resultant Models for Shallow Foundation Systems and Their Implementation in the Analysis of Soil Structure Interactions*, University of Western Australia, Perth.

Cheng, N & Cassidy, MJ 2016a, ‘Combined loading capacity of spudcan footings on loose sand’., *International Journal of Physical Modelling in Geotechnics*, vol. 16, no. 1, pp.31–44.

Cheng, N & Cassidy, MJ 2016b, ‘Development of a force–resultant model for spudcan footings on loose sand under combined loads’., *Canadian Geotechnical Journal*, vol. 53, pp.2014–2029.

Christophersen, HP 1993, ‘‘The non-piled foundation system of the Snorre field’’, *Proc. Offshore Site Invest. Found. Behav., Soc. Underwater tech.* , p.28: 433-447.

Foglia, A, Gottardi, G, Govoni, L & Ibsen, LB 2015, ‘Modelling the drained response of bucket foundations for offshore wind turbines under general monotonic and cyclic loading’., *Applied Ocean Research*, vol. 52, pp.80–91.

Gottardi, G & Butterfield, R 1995, ‘The displacement of a model rigid surface footing on dense sand under general planar loading’., *Soils and Foundations, The Japanese Geotechnical Society*, vol. 35, no. 3, pp.71–82.

Gottardi, G, Houlsby, GT & Butterfield, R 1999, ‘Plastic response of circular footings on sand under general planar loading’., *Géotechnique*, vol. 49, no. 4, pp.453–469.

Govoni, L, Gottardi, G & Gourvenec, S 2010, ‘Centrifuge modelling of circular shallow foundations on sand’., *International Journal of Physical Modelling in Geotechnics*, vol. 10, no. 2, pp.35–46.

Govoni, L, Gourvenec, S & Gottardi, G 2011, ‘A centrifuge study on the effect of embedment on the drained response of shallow foundations under combined loading’., *Géotechnique*, vol. 61, no. 12, pp.1055–1068.

Houlsby, GT 2016, ‘Interactions in offshore foundation design’., *Géotechnique*, vol. 66, no. 10, pp.791–825.Houlsby, GT & Byrne, BW 2005, ‘Design procedures for

installation of suction caissons in sand'., *Geotechnical Engineering,* vol. 158, no. 3, pp.135–144.

Houlsby, GT, Ibsen, LB & Byrne, BW 2005, ''Suction caissons for wind turbines'', *Proc. International Symposium in Offshore Geotechnics,* pp.85-93.

Liu, QB & Lehane, BM 2012, 'The influence of particle shape on the (centrifuge) cone penetration test (CPT) end resistance in uniformly graded granular soils'., *Géotechnique,* vol. 62, no. 11, pp.973–984.

Martin, CM 2003, 'New software for rigorous bearing capacity calculations'., *Proc. International Conference on Foundations,* pp.581–592.

Nova, R & Montrasio, L 1991, 'Settlements of shallow foundations on sand'., *G&echnique,* vol. 41, no. 2, pp.243–256.

Tan, K 1990, *Centrifuge and theoretical modelling of footings on sand,* University of Cambridge, UK.

Tjelta, TI 2015, 'The suction foundation technology'., *Proceeding of the Third International Symposium on Frontiers in Offshore Geotechnics* , pp.85.

Villalobos Jara, FA 2006, *'*Model Testing of Foundations for Offshore Wind Turbines*'*, University of Oxford.

Zhang, Y, Bienen, B & Cassidy, M 2013, 'Development of a combined VHM loading apparatus for a geotechnical drum centrifuge'., *International Journal of Physical Modelling in Geotechnics,* vol. Volume 13, no. 1, p.18.

598 Table 1: Summary of representative work on drained VHM capacity of shallow foundations on sand.

Reference	**Foundation type**	**D (mm)**	**d/D (-)**	**V/A (kPa)**	**Dr (%)**	**g level**	**h_0**	**m_0**	**α**	**β_1**	**β_2**	**t_0**
Gottardi et al. (1999)	flat	100	0	~200	75%	1	0.1213	0.09	-0.2225	1	1	0
Byrne & Houlsby (1999), Byrne (2000)	flat	100	0	~127	95%	1	0.11	0.08	0.06	1	1	0
	caisson		0.166				0.15	0.074	-0.25			
			0.33				0.17	0.074	-0.75			
			0.66				0.13	0.09	-0.93			
Byrne & Houlsby (2001)	flat	150	0	~90	Loose (carbonate)	1	0.154	0.094	-0.25	0.82	0.82	0
Houlsby & Cassidy (2002)	flat	100	0	~200	75%	1	0.116	0.086	-0.2	0.9	0.9	0
Bienen et al. (2006)	flat	150	0	~50	5%	1	0.122	0.075	-0.112	0.76	0.76	0
Cassidy (2007)	flat	60	0	~300	45%	100	*[1]	*	*	*	*	0
Villalobos et al. (2009)	caisson	50.9	0.5	~300	23%	1	0.279	0.128	-0.84	0.89	0.99	0.12
			1				0.235	0.124	-0.87	0.93	0.99	0.16
Govoni et al. (2011)	flat	30, 50	0	~500	50%	100	0.154	0.094	-0.25	0.82	0.82	0
	buried		0.5				NA	NA	NA	NA	NA	0

[1] Fitting coefficients refers to Byrne & Houlsby (2001) and Bienen et al. (2006)

			1				NA	NA	NA	NA	NA	v_t^2=0.085
Cheng & Cassidy (2016)	spudcan	60	0	~300	35%	100	0.113	0.096	-0.248	0.71	0.99	0
	skirted		0.133	~500	35%		0.21	0.097	-0.51	0.77	0.96	0
					90%		0.37	0.15	0.5	0.81	0.99	0
This study	skirted	50	0.25	~100 - 500	30%	100						[3]
			0.5									

599

[2] parameter which accounts for a non-linear expansion of the yield surface with the embedment of the foundation and used to fit the data close to the origin (Govoni et al. 2011)

600 Table 2: Material properties of sand used in centrifuge tests (Liu & Lehane 2012).

Property	**Value**
G_s	2.650
D_{50} (mm)	0.150
e_{min}	0.449
e_{max}	0.747
ϕ_{cv} (º)	31

601

Table 3: Summary of swipe tests (in prototype dimensions).

Type of tests		Test name		Target		Measured			Swipe parameters		
			d/D	V/A (kPa)	w_0 (m)	V_0 (MN)	w_0 (m)	w_0/D (-)	u/Dθ (rad^{-1})	u (m)	θ (°)
Vertical penetration		VP_0.25	0.25	-	-		-	-	-	-	-
		VP_0.5	0.5	-	-		-	-	-	-	-
Load-unload		LU_0.25	0.25	-	-		-	-	-	-	-
		LU_0.5	0.5	-	-						
SWIPE TESTS	**ARRANGEMENTS FOR JACKET STRUCTURES**	**SW1**	0.25	~500	~1.7	**11.85**	1.92	0.38	∞	0.9	0
		SW2	0.25	~500	~1.7	**11.6**	1.91	0.38	-1.15	0.9	-9
		SW3	0.25	~500	~1.7	**9.14**	1.84	0.37	-0.1	0.09	-9
		SW4	0.25	~500	~1.7	**10.65**	1.84	0.37	1.15	-0.9	-9
		SW9	0.5	~500	~2.8	**11.07**	2.91	0.58	∞	0.9	0
		SW10	0.5	~500	~2.8	**9.81**	2.91	0.58	-1.15	0.9	-9
		SW11	0.5	~500	~2.8	**12.16**	2.96	0.59	-0.1	0.09	-9
		SW12	0.5	~500	~2.8	**9.61**	2.90	0.58	1.15	-0.9	-9
	MONOPOD FOR WIND TUBINE	SW5	0.25	~100	~1.3	**2.89**	1.31	0.26	∞	0.9	0
		SW6	0.25	~100	~1.3	**2.30**	1.31	0.26	-1.15	0.9	-9
		SW7	0.25	~100	~1.3	**4.1**	1.34	0.27	-0.1	0.09	-9
		SW8	0.25	~100	~1.3	**2.84**	1.32	0.26	1.15	-0.9	-9
		SW13	0.25	~100	~2.5	**4.87**	2.66	0.53	∞	0.9	0
		SW14	0.25	~100	~2.5	**5.83**	2.70	0.54	-1.15	0.9	-9
		SW15	0.25	~100	~2.5	**5.5**	2.69	0.53	-0.1	0.09	-9
		SW16	0.25	~100	~2.5	**3.83**	2.67	0.53	1.15	-0.9	-9

607 Table 4: Details of vertical penetration tests (after Villalobos 2006)

Test name	**d/D**	**Dr (%)**	**w_0/D**	**V_0/A (kPa)**
FV62	0.26	26	0.25	4.00
FV21	0.26	40	0.26	3.00
FV63	0.51	26	0.51	6.00
FV22	0.51	40	0.49	5.00

608

609

610 Table 5: Yield surface parameters (overall fit) for Eq. 1

Parameters	**Value**	**Description**
h_0	0.16	Size in the horizontal plane
m_0	0.13	Size in the moment plane
α	0.6	Eccentricity
β_1	1	Shaping parameter
β_2	1	Shaping parameter

611

612

613

LIST OF FIGURES:

Figure 15: Experimental results with VHM yield surface, overall fit for Houlsby and Byrne parameters (2001), a) d/D= 0.25, b) d/D = 0.5.

Figure 16: Experimental results with VHM yield surface, overall fit for Villalobos parameters (2006)), a) d/D= 0.25, b) d/D = 0.5.

Figure 17: Experimental results with VHM yield surface (overall fit), a) d/D = 0.25, b) d/D = 0.5.

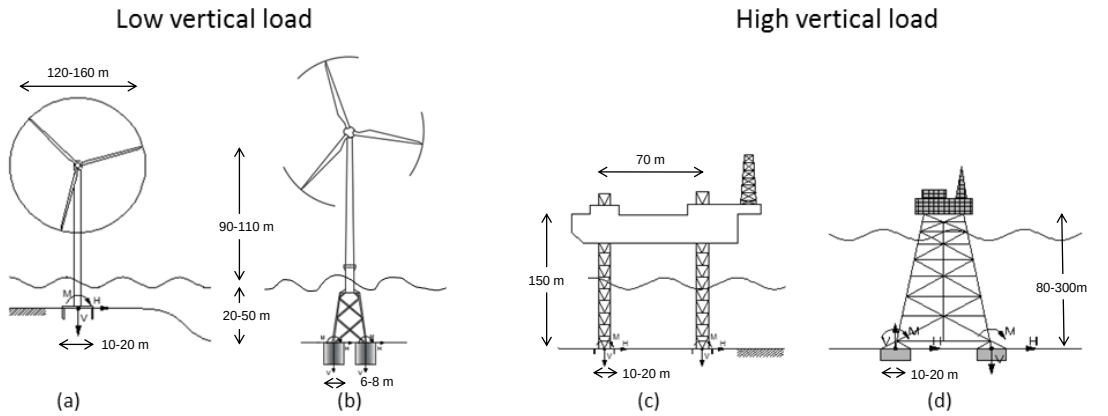

Figure 1**:** Offshore energy infrastructure supported by skirted foundations as a) monopod, b and d) jacket with multiple foundations, c) jack-up with typically three foundation.

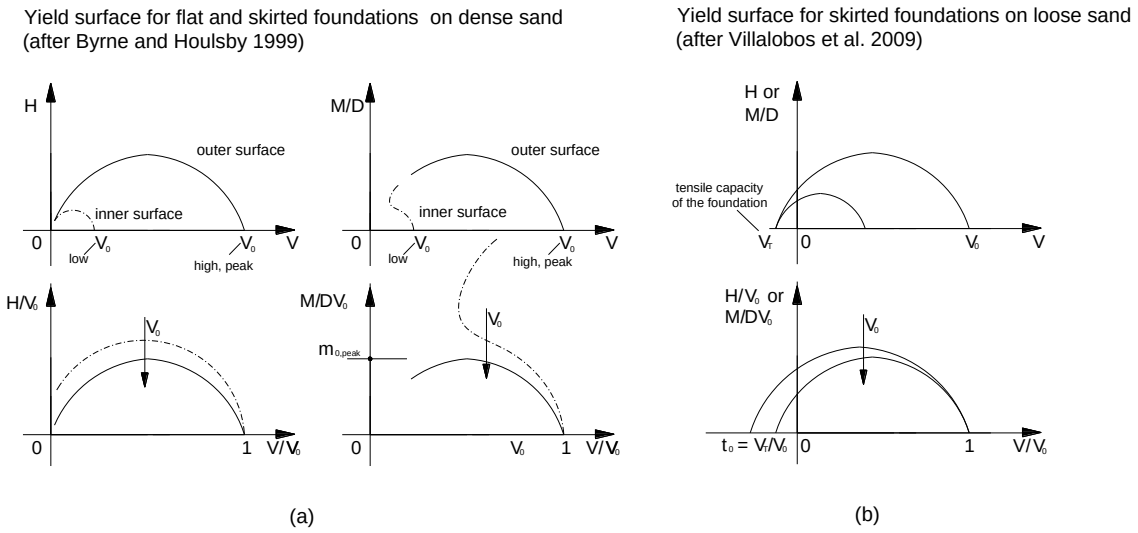

Figure 2**:** Schematic representations of the yield surface for skirted foundations on sand in drained conditions based on 1g experiments: a) shape and size governed by the mobilised stress level and M/(HD) ratio and b) allowance for horizontal and moment capacity in the tensile range of vertical load.

654

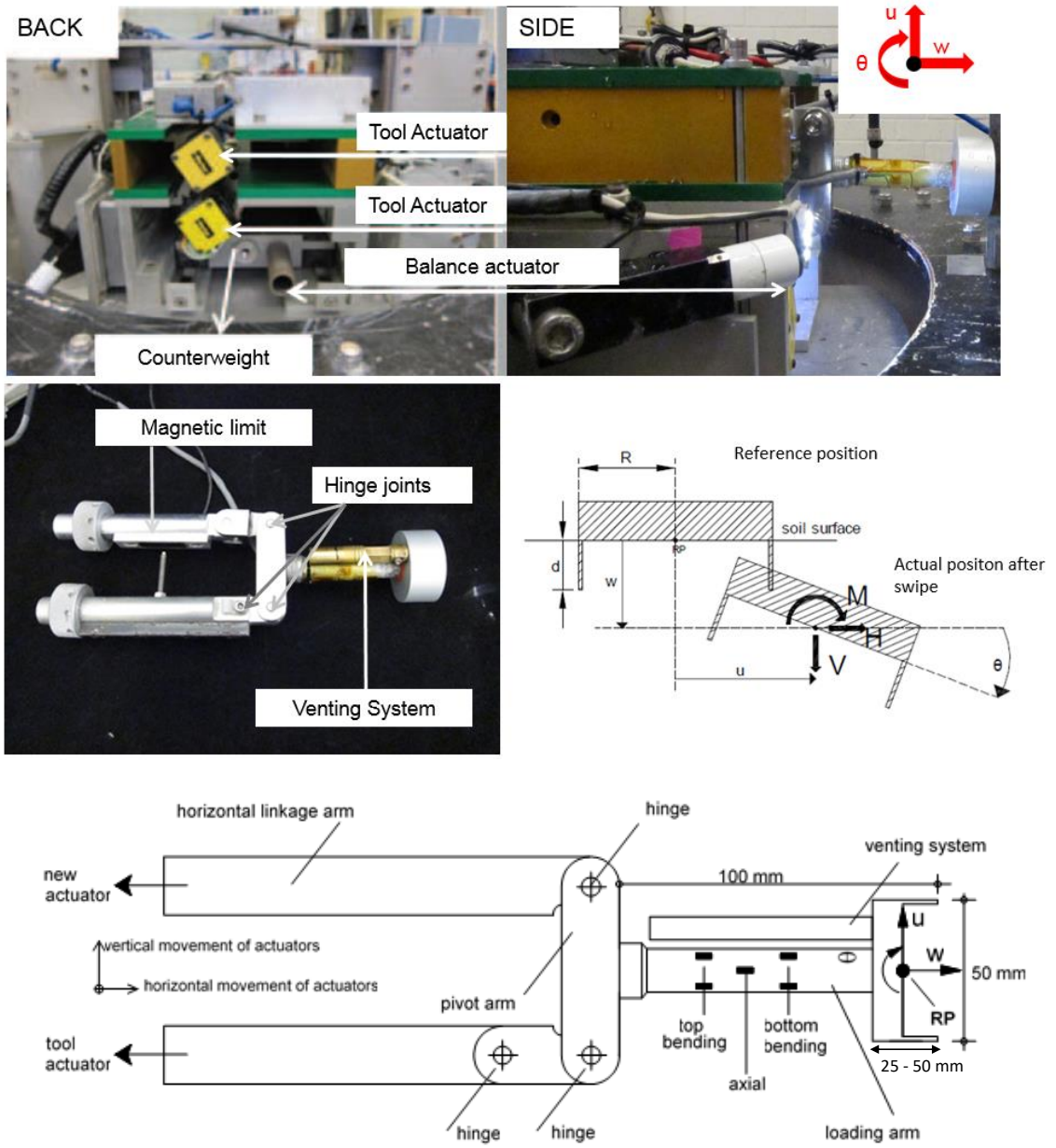

655

656

657 Figure 3**:** Centrifuge set-up, foundation model and sign convention.

658

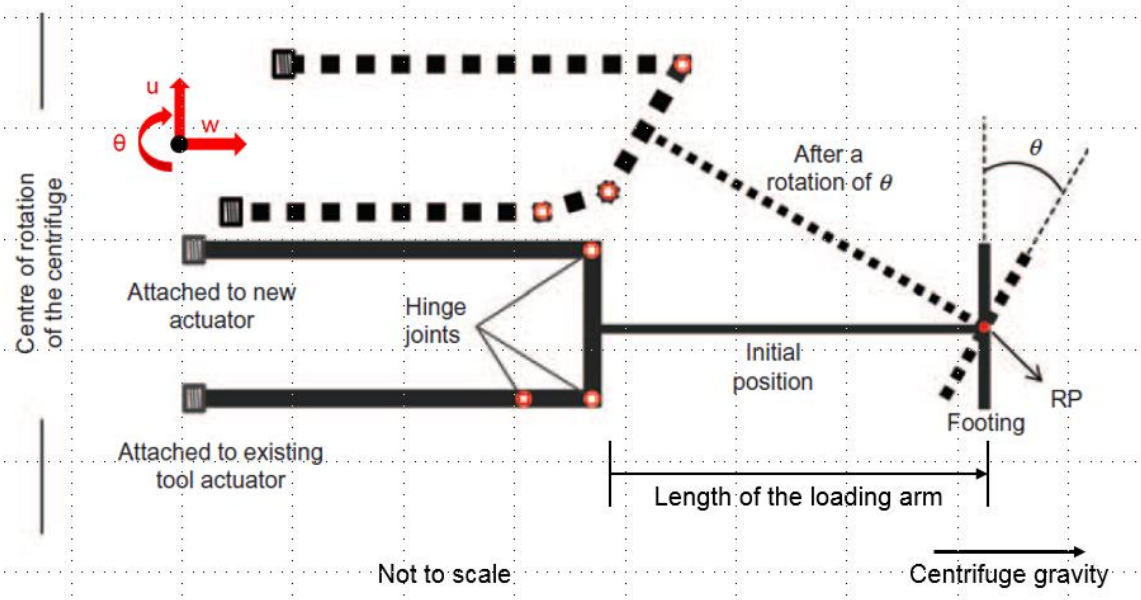

659

660 Figure 4: Movements of the VHM actuator that result in rotation about the reference point

661 (RP) after Zhang et al. (2013).

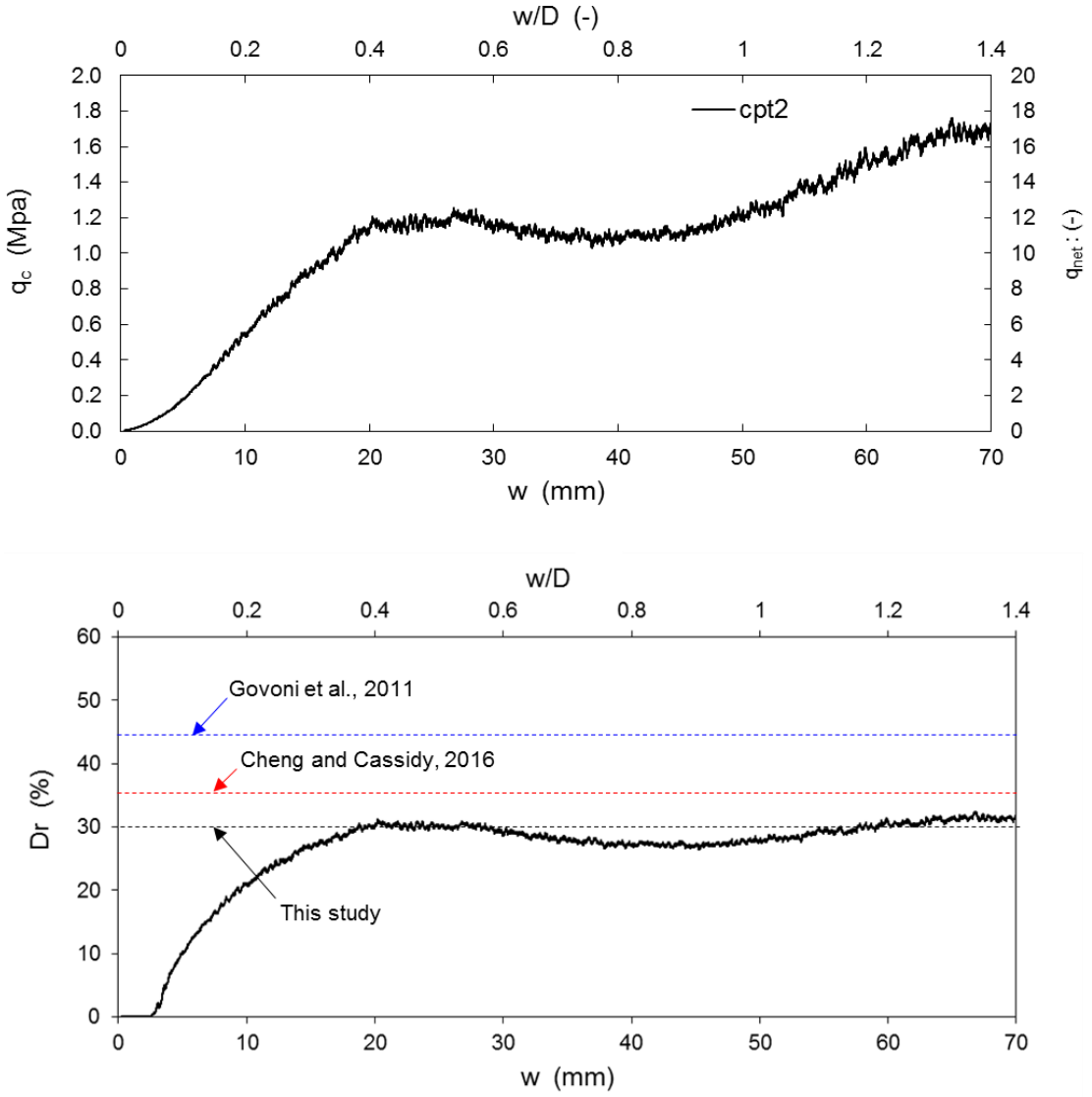

Figure 5 Characterization of sand sample from miniature CPT, in terms of a) measured and net cone resistance, q_c and q_{net} and b) relative density D_r.

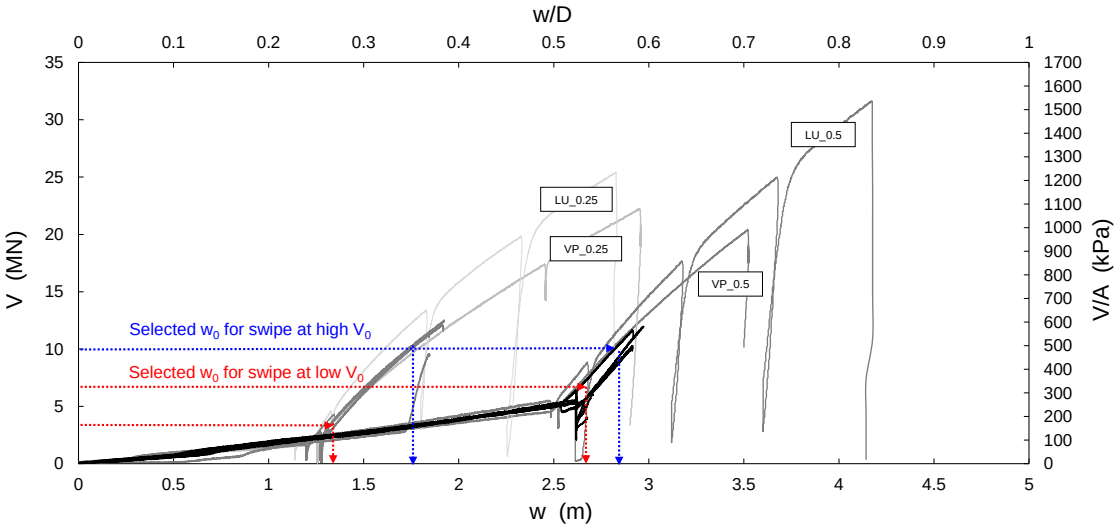

(a)

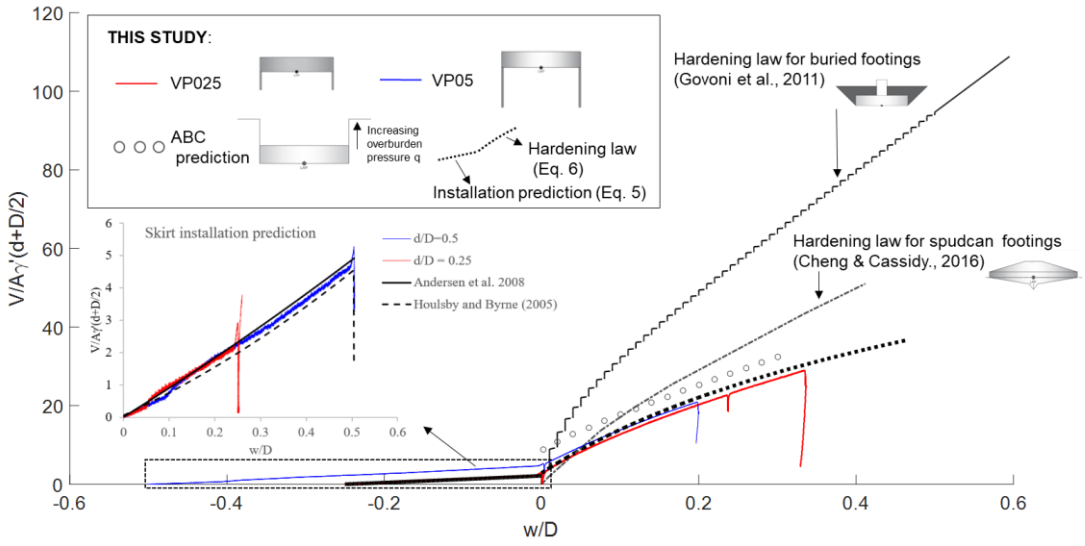

(b)

Figure 6: Vertical load-penetration curves, a) in prototype dimensions, b) normalised.

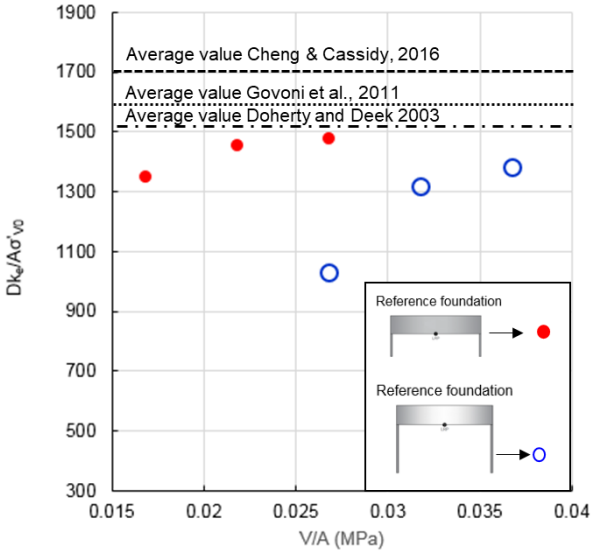

Figure 7: Vertical unloading stiffness.

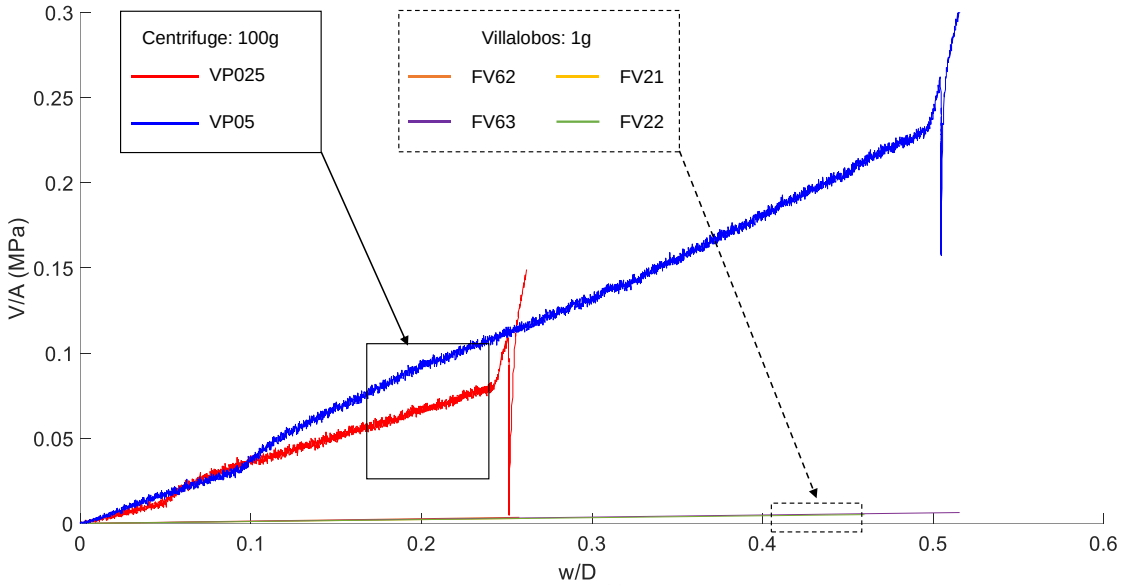

(a)

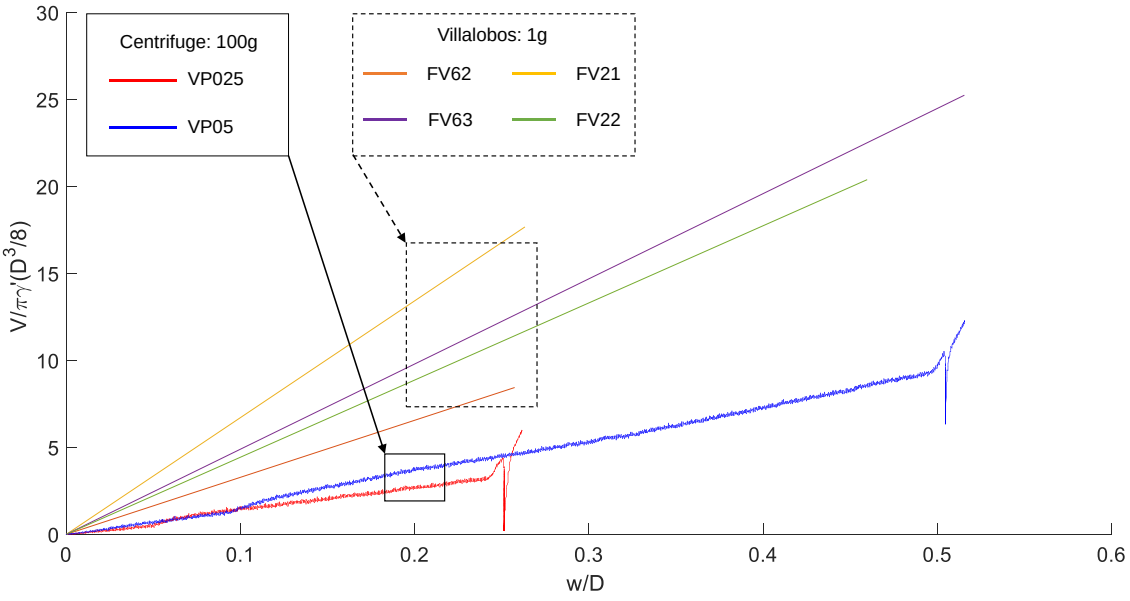

(b)

Figure 8: Normalised load-penetration curves.

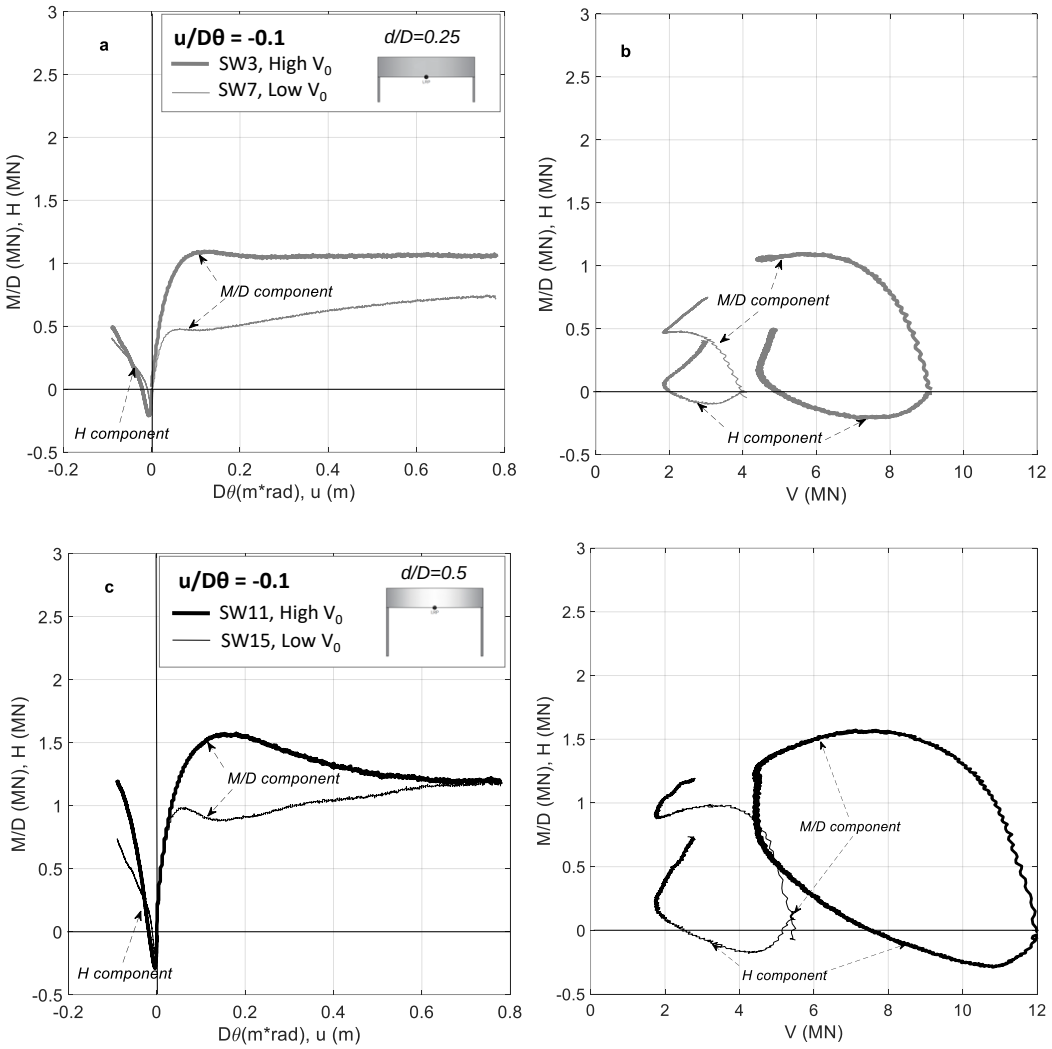

681 Figure 9: Swipe test results for a test dominated by moment.

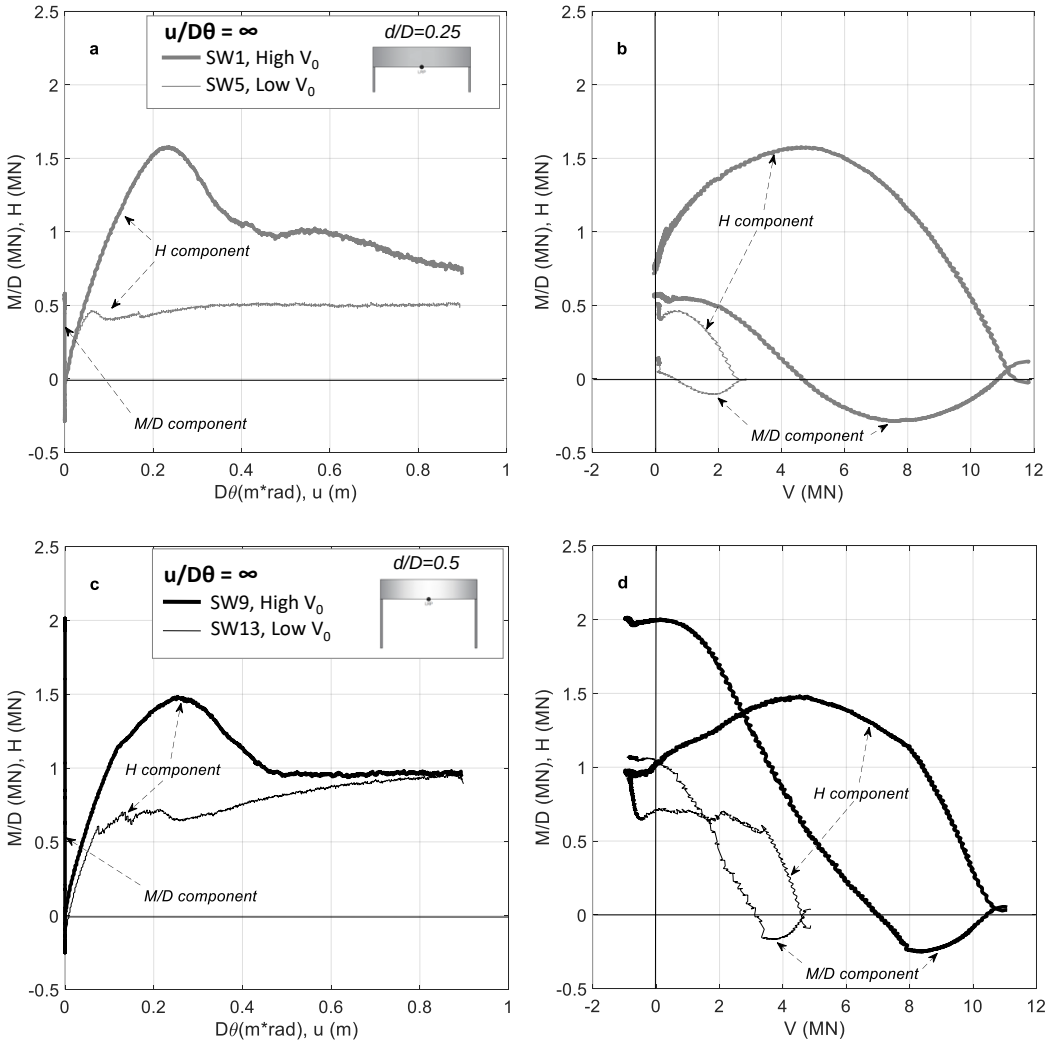

Figure 10: Swipe test results for a test dominated by horizontal load.

682

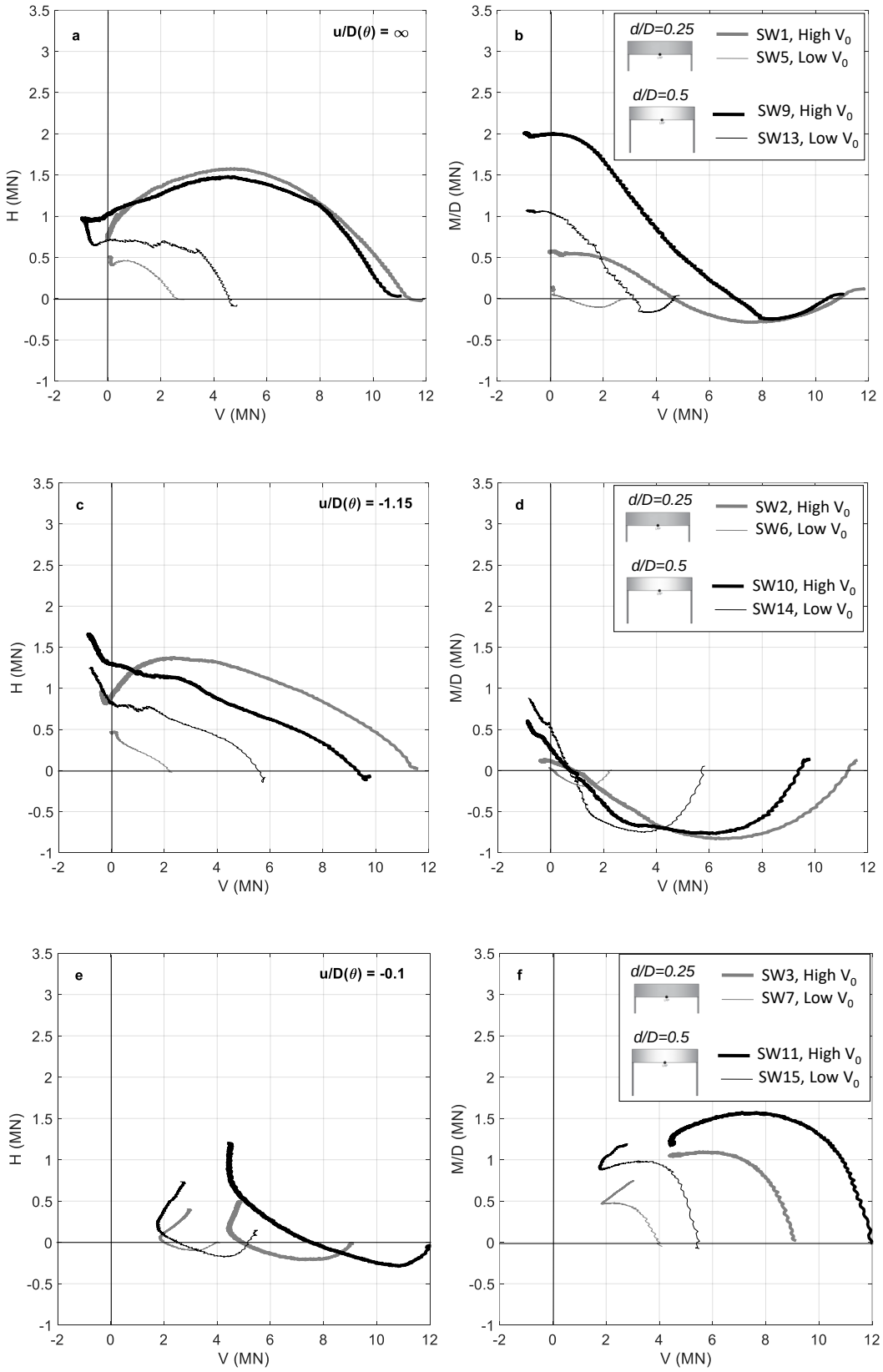
a
u/D(θ) = ∞
b
d/D=0.25
SW1, High V0
SW5, Low V0
d/D=0.5
SW9, High V0
SW13, Low V0
c
u/D(θ) = -1.15
d
d/D=0.25
SW2, High V0
SW6, Low V0
d/D=0.5
SW10, High V0
SW14, Low V0
e
u/D(θ) = -0.1
f
d/D=0.25
SW3, High V0
SW7, Low V0
d/D=0.5
SW11, High V0
SW15, Low V0
H (MN)
M/D (MN)
V (MN)

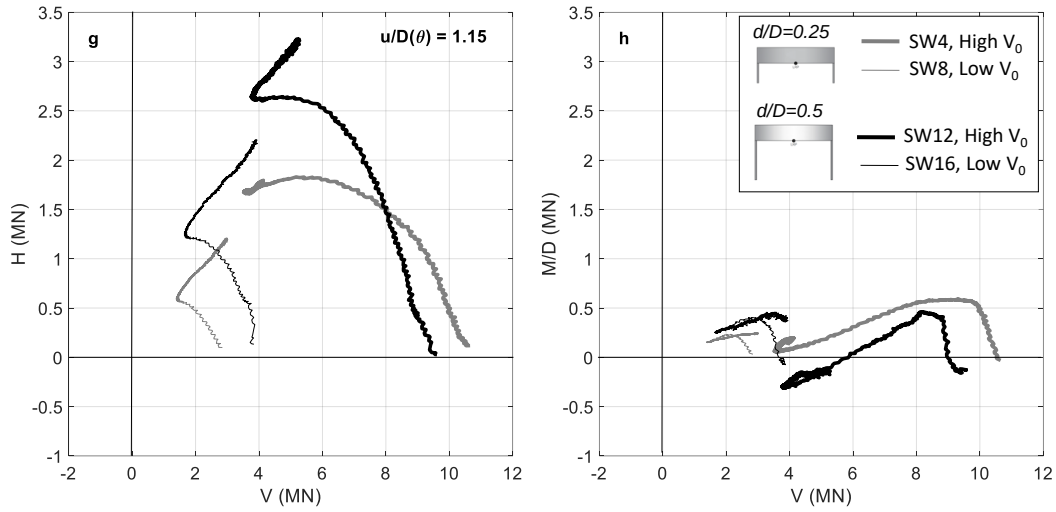

Figure 11: Results of all swipe tests in the a) VH, b) VM/D planes.

683

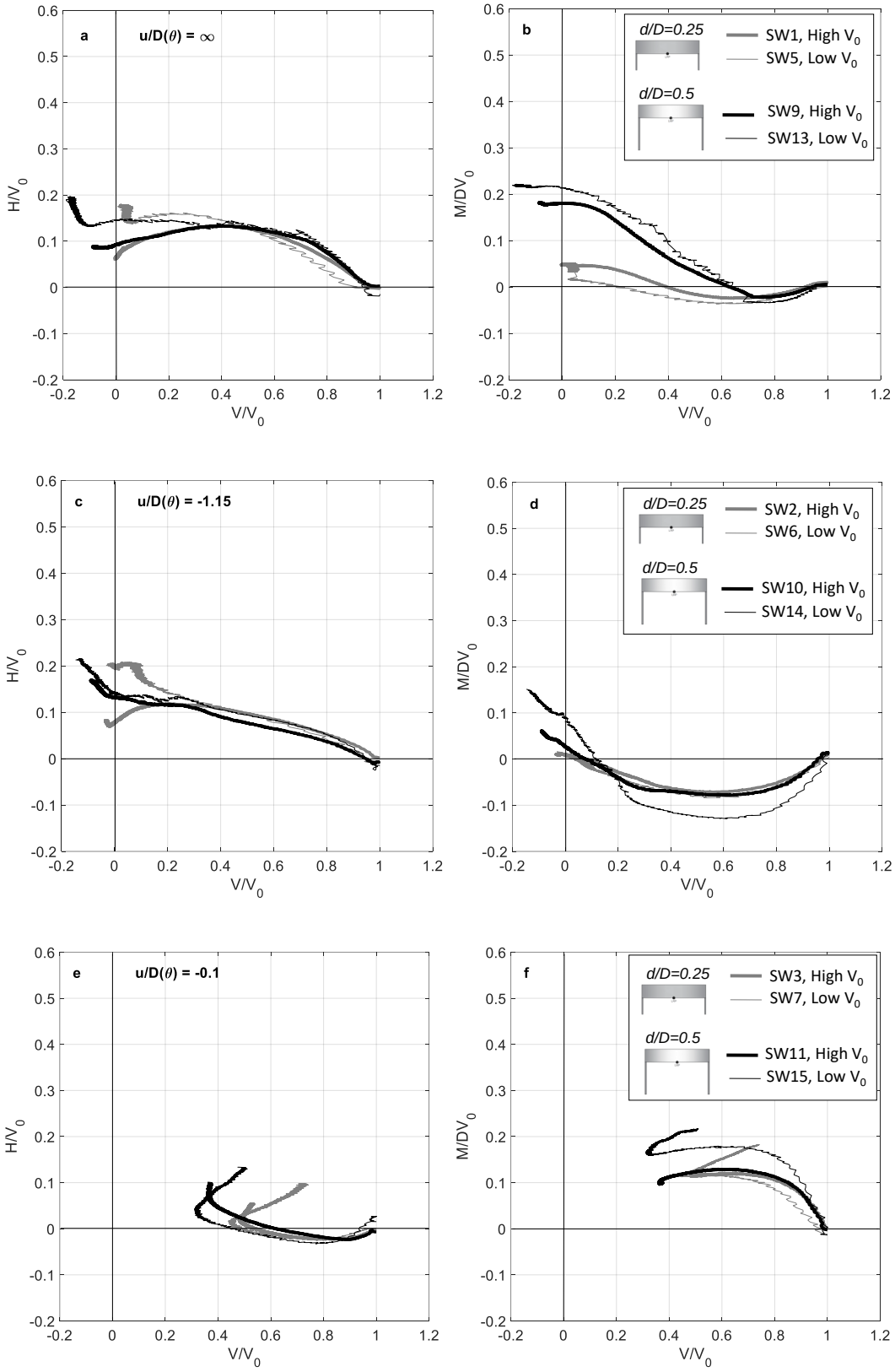
a
u/D(θ) = ∞
b
d/D=0.25
SW1, High V0
SW5, Low V0
d/D=0.5
SW9, High V0
SW13, Low V0
c
u/D(θ) = -1.15
d
d/D=0.25
SW2, High V0
SW6, Low V0
d/D=0.5
SW10, High V0
SW14, Low V0
e
u/D(θ) = -0.1
f
d/D=0.25
SW3, High V0
SW7, Low V0
d/D=0.5
SW11, High V0
SW15, Low V0
H/V0
M/DV0
V/V0

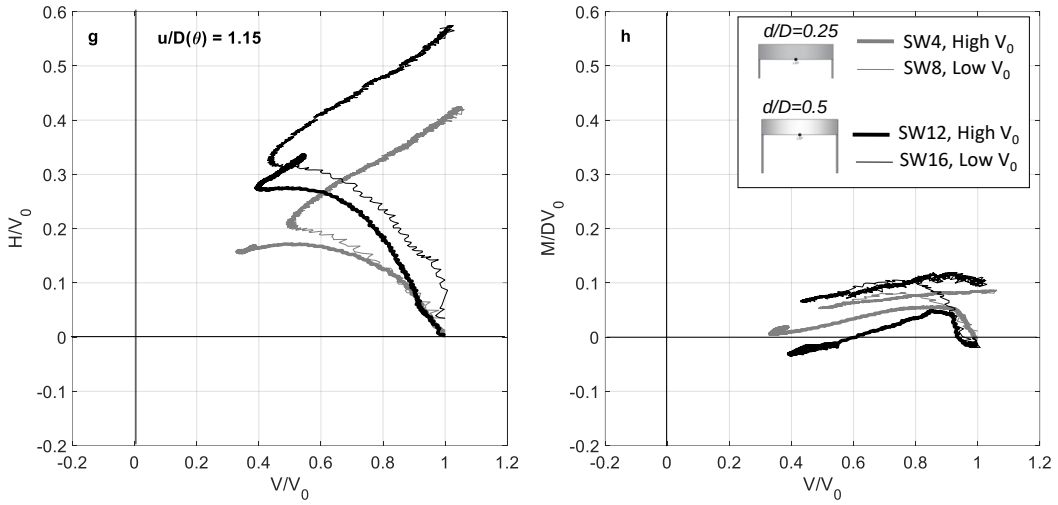

Figure 12: Results of all swipe tests in the a) H/V_0 vs V/V_0, b) M/DV_0 vs V/V_0 planes.

684

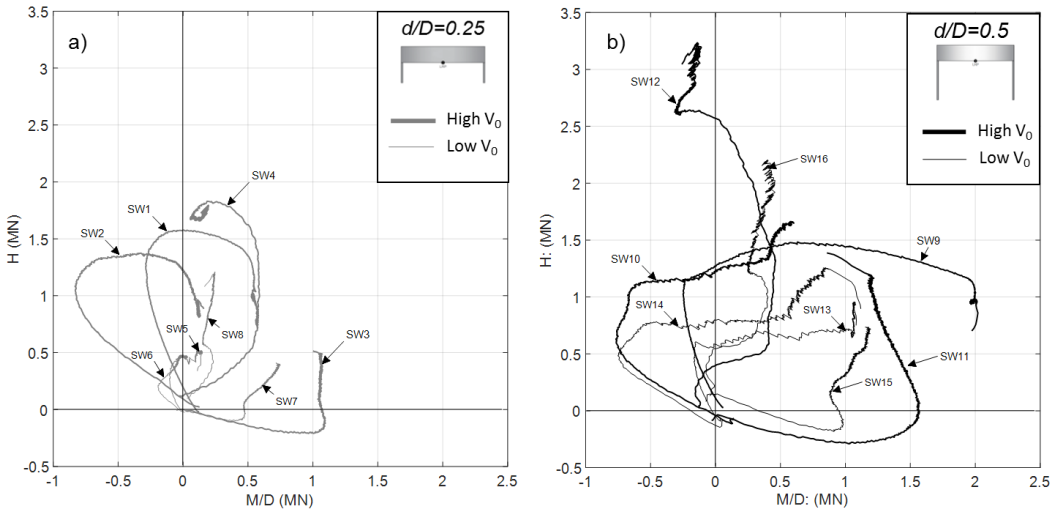

685

686 Figure 13: Result of all swipe tests in the M/D vs H plane in prototype units for a) d/D =
687 0.25 and b) d/D = 0.5.

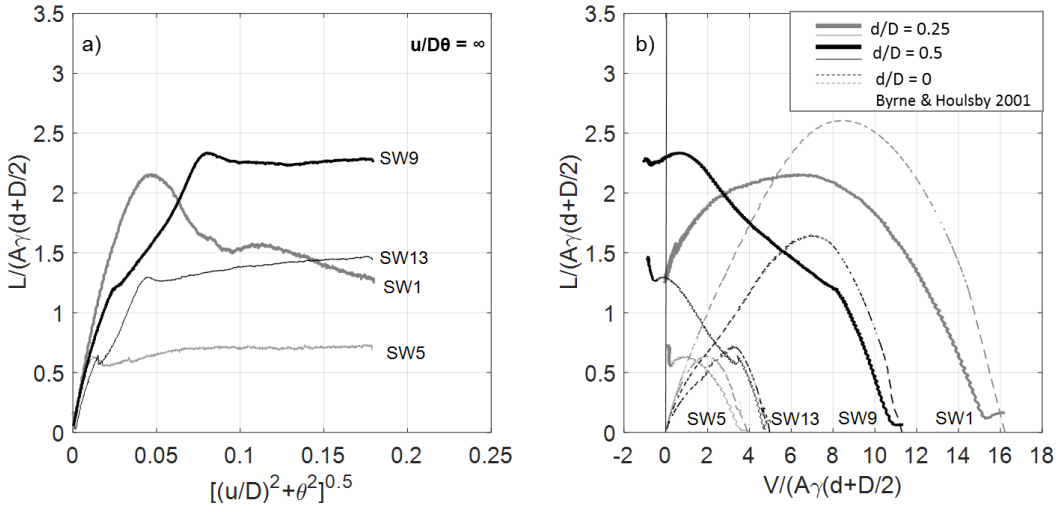

688

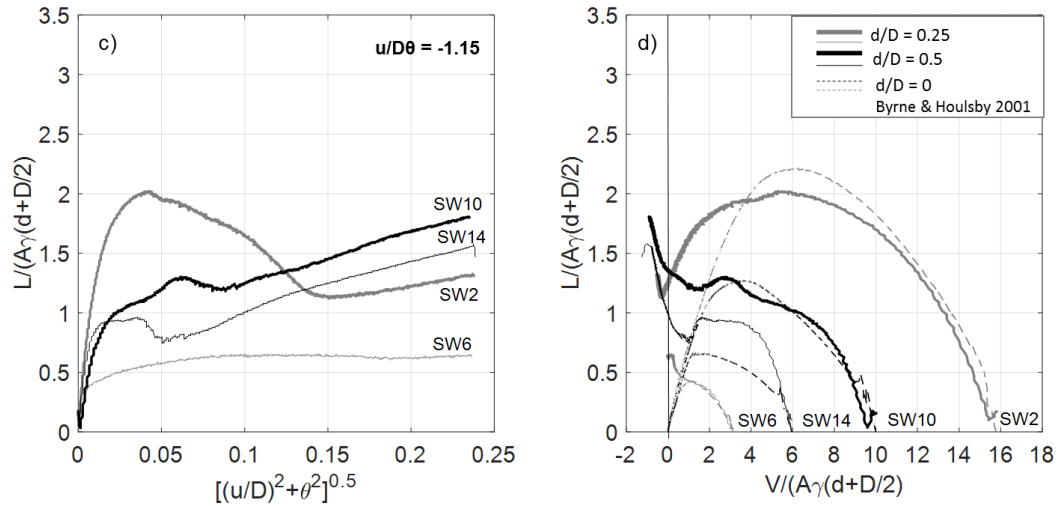

689

690

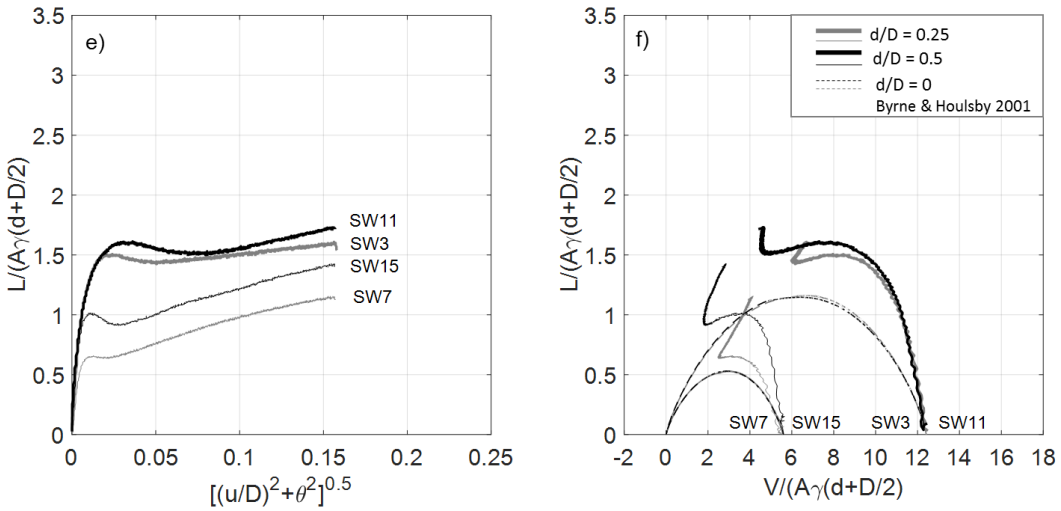

691

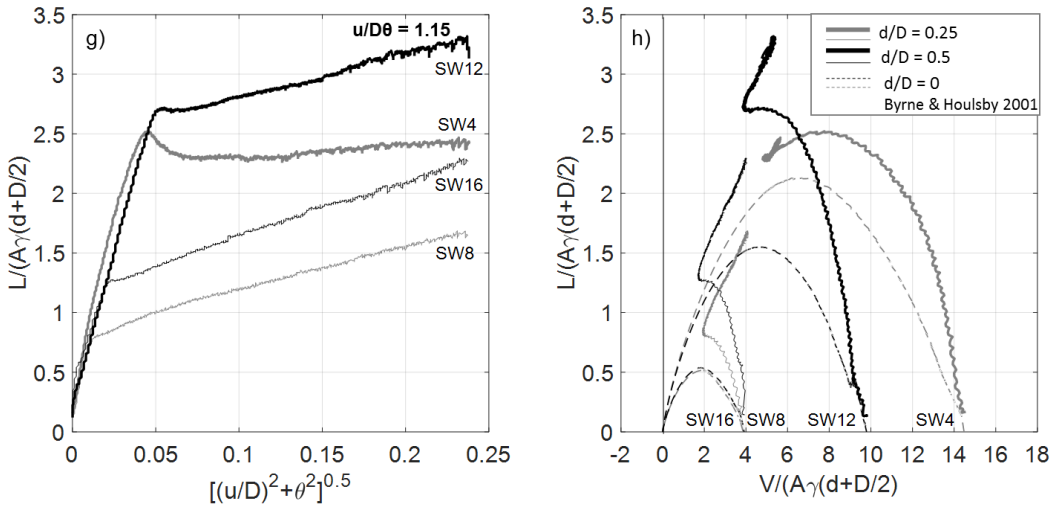

Figure 14: Result of all swipe tests in the a) [(u/D)2+θ2]0.5 vs L/A γ'(d+D/2), b) V/A γ'(d+D/2) : L/A γ'(d+D/2) plane, compared with eq. 1 for surface foundations (Byrne & Houlsby 2001).

Byrne & Houlsby (2001)				
h_0	m_0	α	β_1	β_2
0.154	0.095	-0.25	0.82	0.82

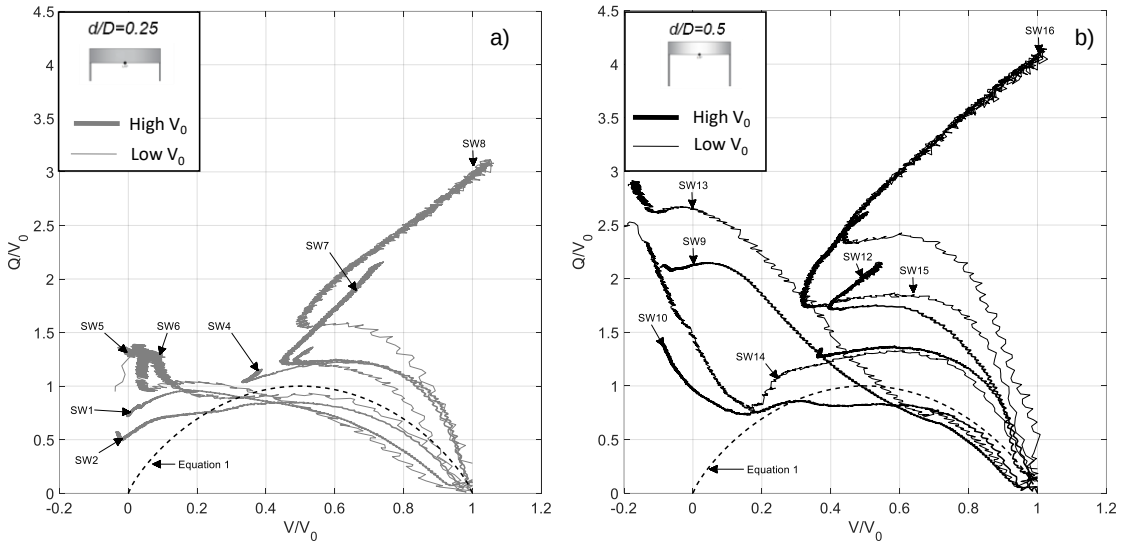

Figure 15: Experimental results with VHM yield surface, overall fit for Byrne and Houlsby parameters (2001), a) d/D= 0.25, b) d/D = 0.5.

Villalobos					
h0	m0	α	β1	β2	to
0.279	0.128	-0.84	0.89	0.99	0.12

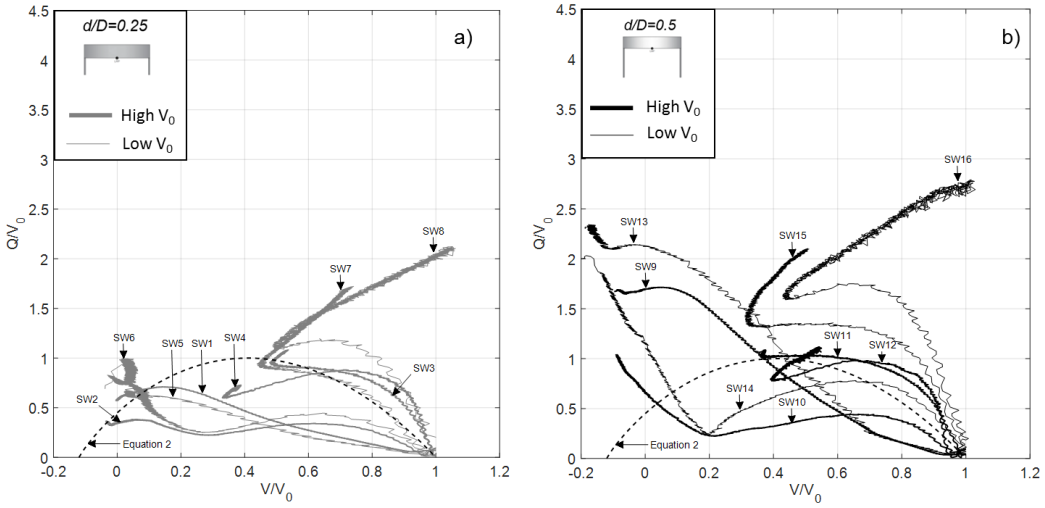

Figure 16: Experimental results with VHM yield surface, overall fit for Villalobos parameters (2006)), a) d/D= 0.25, b) d/D = 0.5.

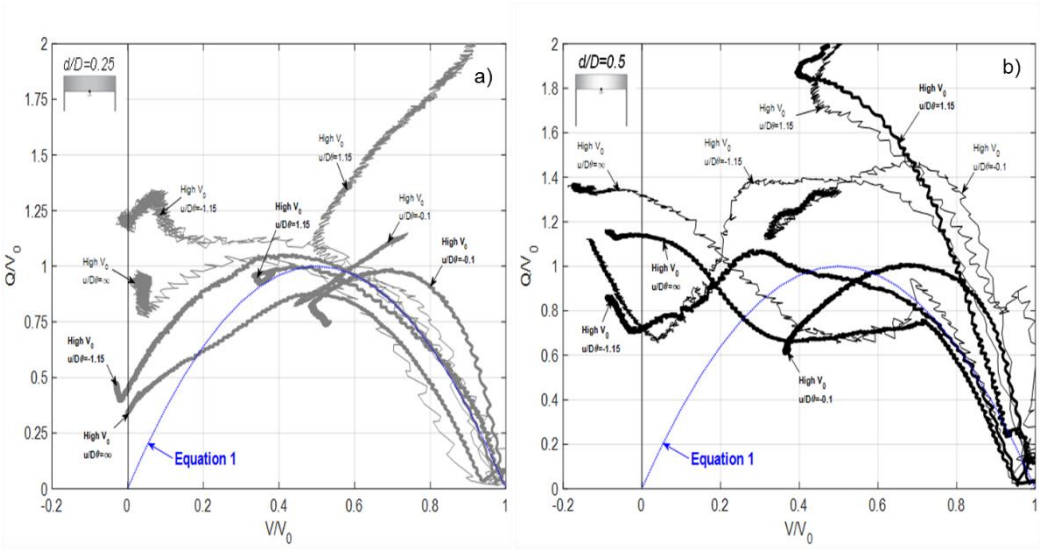

Figure 17: Experimental results with VHM yield surface (overall fit), a) d/D = 0.25, b) d/D = 0.5.